

# Primary and secondary red bed magnetization constrained by fluvial intraclasts

Nicholas L. Swanson-Hysell<sup>1</sup>, Luke M. Fairchild<sup>1</sup>, Sarah P. Slotznick<sup>1</sup>

<sup>1</sup>Department of Earth and Planetary Science, University of California, Berkeley, CA, USA

## Key Points:

- Red siltstone intraclasts reveal two ancient magnetizations held by hematite – one acquired before redeposition and the other after burial
- Fine-grained hematite spans from superparamagnetic to single domain leading to a wide range of unblocking temperatures and coercivities
- Detrital hematite thermally unblocks in a narrow high-temperature range that can be isolated through high-resolution thermal demagnetization

## This paper should be cited as:

Swanson-Hysell, N. L., Fairchild, L. M., and Slotznick, S. P. (2019). Primary and secondary red bed magnetization constrained by fluvial intraclasts. *Journal of Geophysical Research: Solid Earth*, 124. <https://doi.org/10.1029/2018JB017067>

## Abstract

The magnetization of hematite-bearing sedimentary rocks provides critical records of geomagnetic reversals and paleogeography. However, the timing of hematite remanent magnetization acquisition is typically difficult to constrain. While detrital hematite in sediment can lead to a primary depositional remanent magnetization, alteration of minerals through interaction with oxygen can lead to the post-depositional formation of hematite. In this study, we use exceptionally-preserved fluvial sediments within the 1.1 billion-year-old Freda Formation to gain insight into the timing of hematite remanence acquisition and its magnetic properties. This deposit contains siltstone intraclasts that were eroded from a coexisting lithofacies and redeposited within channel sandstone. Thermal demagnetization, petrography and rock magnetic experiments on these clasts reveal two generations of hematite. One population of hematite demagnetized at the highest unblocking temperatures and records directions that rotated along with the clasts. This component is a primary detrital remanent magnetization. The other component is removed at lower unblocking temperatures and has a consistent direction throughout the intraclasts. This component is held by finer-grained hematite that grew and acquired a chemical remanent magnetization following deposition resulting in a population that includes superparamagnetic nanoparticles in addition to remanence-carrying grains. The data support the interpretation that magnetizations of hematite-bearing sedimentary rocks held by  $>400$  nm grains that unblock close to the Néel temperature are more likely to record magnetization from the time of deposition. This primary magnetization can be successfully isolated from co-occurring authigenic hematite through high-resolution thermal demagnetization.

## 1 Introduction

The magnetizations of hematite-bearing sedimentary rocks known as “red beds” have provided ample opportunities for Earth scientists to gain insight into the ancient geomagnetic field and the paleogeographic positions of sedimentary basins. However, with these opportunities has come much scientific debate, leading to what has been referred to as the “red bed controversy” (Butler, 1992; Beck et al., 2003; Van Der Voo & Torsvik, 2012). This controversy stems from the reality that hematite within sedimentary rocks can have two sources: 1) detrital grains that are within the sediment at the time of deposition; and 2) grains that grow *in situ* after the sediments have been deposited.

How does one constrain the relative age of hematite within sedimentary rocks? Many of the traditional paleomagnetic field tests are unable to differentiate between primary versus diagenetic remanence. For example, a structural fold test can constrain that a remanence direction was obtained prior to folding, but millions of years have typically passed between the deposition of a sediment and such tectonic tilting. Dual-polarity directions through a sedimentary succession are commonly interpreted as providing assurance that the remanence records primary or near-primary magnetization; however, hematite growth could occur significantly after deposition during a protracted period over which the geomagnetic field was in both reversed and normal polarities. Petrographic investigations are valuable, but it can be difficult to ascertain how much the petrographically observed hematite contributes to the magnetization and to unambiguously interpret whether observed grains are detrital or not (e.g. (Elmore & Van der Voo, 1982)). A common approach to classify hematite grains within red beds is into a fine-grained pigmentary population, typically interpreted to have formed within the sediment, and a coarser-grained population that has been referred to in the literature as “specularite” (Butler, 1992; Van Der Voo & Torsvik, 2012). Tauxe et al. (1980) showed that sediments with abundant red pigmentary hematite in the Miocene Siwalik Group had lower thermal unblocking temperatures than grey samples dominated by a coarser-grained phase of specular hematite. An additional approach taken by Tauxe et al. (1980), and other workers going back to

the work of Collinson (1965), is to preferentially remove fine-grained pigmentary hematite through prolonged immersion in concentrated HCl acid. Paired chemical and thermal demagnetization have been interpreted to show that removal of pigmentary hematite coincides with removal of hematite associated with lower unblocking temperatures. These data support the interpretation that coarser grains that are more resistant to dissolution in acid correspond with those that carry remanence to the highest unblocking temperatures (Tauxe et al., 1980; Bilardello & Kodama, 2010a); although simultaneous dissolution of fine and coarser hematite can occur (Jiang et al., 2017). Observations such as these have led to the practice of defining the characteristic remanent magnetization from hematite-bearing sediments as that held by the highest unblocking temperatures (Van Der Voo & Torsvik, 2012). Additional lines of evidence in numerous successions have supported this approach. For example, in the well-studied Carboniferous Mauch Chunk Formation of Pennsylvania, remanence removed up to  $\sim$ 660°C has uniform polarity and fails a fold test while the component removed upwards of 670°C is dual-polarity, was acquired before folding, and is interpreted as a primary magnetization (Kent & Opdyke, 1985; DiVenere & Opdyke, 1991). Nevertheless, the primary versus secondary nature of micron-scale “specularite” grains that likely carry this remanence has been one of the largest sources of contention in the “red bed controversy” (Van Houten, 1968; Tauxe et al., 1980; Butler, 1992; Van Der Voo & Torsvik, 2012).

What is needed to most confidently address the timing of remanence acquisition is a process that reorients the sediment before it has been fully lithified. Two such processes are: 1) syn-sedimentary slumping wherein coherent sediment is reoriented through soft-sediment folding in the surface environment and 2) intraclasts comprised of the lithology of interest that have been liberated and redeposited within the depositional environment. Sediments that have undergone reorienting processes within the depositional environment can provide significant insight into whether magnetization was acquired before or after reorientation.

Tauxe et al. (1980) studied 7 cobble-sized clasts within the Siwalik Group that were interpreted to have formed by cut-bank collapse and discovered that their magnetic remanence was acquired prior to clast reorientation. Molina-Garza et al. (1991) observed dispersed magnetization directions in sandstone and siltstone clasts within the Triassic Moenkopi and Chinle formations in New Mexico and interpreted the characteristic remanence to be a detrital or early chemical remanence. An investigation by Purucker et al. (1980) on red beds also of the Triassic Moenkopi Formation of Arizona used multiple such syn-sedimentary processes to gain insight into hematite acquisition. In their study, an intraformational landslide deposit with isoclinal folds of hematite-bearing claystone revealed non-uniform directions when analyzed at a single thermal demagnetization step of 650°C that cluster better when corrected for their tilt, leading to a primary interpretation for their remanence. Scatter was also observed in intraformational conglomerate clasts weathered out of an underlying unit at the single thermal demagnetization step of 630°C. However, the lack of principal component analysis makes it difficult to evaluate the coherency of the directions. Complicating matters, Larson and Walker (1982) analyzed shale rip-up clasts in the same Moenkopi Formation and used the fact that similar remanence directions were removed between clasts during thermal demagnetization up to 645°C as support for the hypothesis that red beds rarely reflect the geomagnetic field at the time of deposition. Evaluating the robustness of this result, as well as the varying results of similar field tests conducted by Liebes and Shive (1982) on the Chugwater and Moenkopi formations, is hindered by the cessation of thermal demagnetization before the Néel temperature of hematite and the lack of principal component analysis. These limitations are found in many studies from this era of research, when the red bed controversy was particularly fervent, as the work predates the widespread application of principal component analysis in conjunction with systematic progressive thermal demagnetization (Kirschvink, 1980; Van Der Voo & Torsvik, 2012). Using such methods, Opdyke and DiVenere (2004) analyzed 20 red siltstone rip-up clasts from the Mauch

Chunk Formation and found that the remanence component that unblocks above 650°C and passes a structural fold test was reoriented with the rip-up clasts providing strong evidence for a syndepositional or early post-depositional origin of the hematite.

In this study, we investigate cm-scale siltstone intraclasts within the ca. 1.1 Ga Freda Formation that were eroded by fluvial processes and redeposited amongst cross-stratified sandstones (Fig. 1). High-resolution thermal demagnetization data on these clasts constrain the timing of hematite acquisition by revealing a primary component that formed prior to the erosion of the clasts within the depositional environment and a secondary component that formed following their redeposition. Rock magnetic experiments constrain the magnetic mineralogy and provide additional insights into the grain size of the hematite populations that hold these remanences.

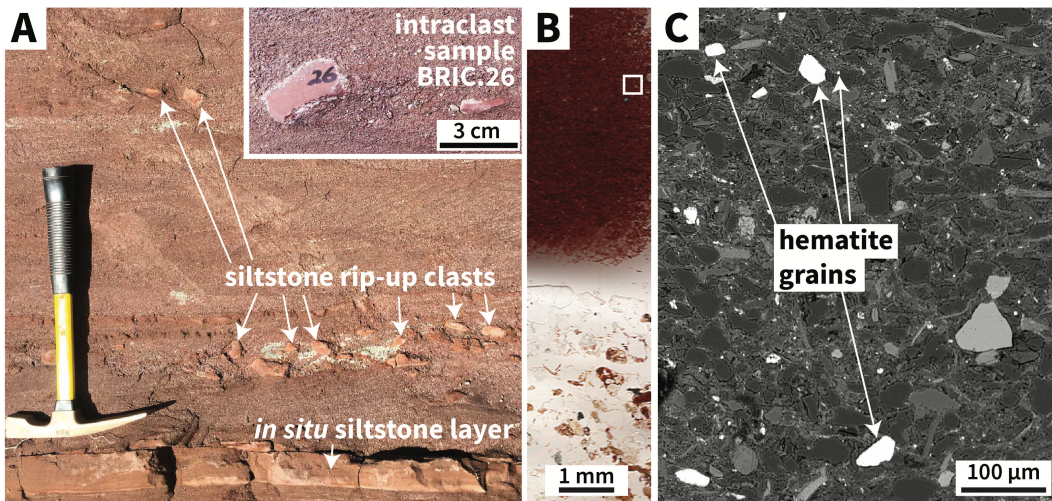


**Figure 1.** A: Siltstone intraclasts within the Freda Formation. The field photo shows an intact layer of siltstone below the hammer head which is topped by a bed of trough cross-stratified coarse-grained sandstone with horizons of siltstone intraclasts. The hammer is 40 cm long. The inset photo is of an individual intraclast that was sampled as BRIC.26. B: A scan of a 30  $\mu\text{m}$ -thick thin section of the BRIC.26 intraclast (upper half of image) and the coarse sand matrix (lower half of image). The red color of the intraclast is due to pigmentary hematite. C: Backscatter electron image of the siltstone clast from the region of the white box in B. The light-colored detrital grains that are labeled with arrows (light due to iron's high atomic number) were confirmed to be hematite through electron backscatter diffraction.

The ~5 km thick Freda Formation was deposited in the North American Midcontinent Rift as it was thermally subsiding following the cessation of widespread magmatic activity (Cannon, 1992). The fluvial sediments of the Freda Formation are part of the Orono Group and were conformably deposited following the deposition of the alluvial Copper Harbor Conglomerate and the lacustrine Nonesuch Formation (Ojakangas et al., 2001; Slotznick et al., 2018). Abundant fine-grained red siltstones within the Freda Formation have a well-behaved magnetic remanence dominated by hematite (Henry et al., 1977). A maximum age constraint on the Freda Formation of  $1085.57 \pm 0.25/1.3$  Ma ( $2\sigma$  analytical/analytical + tracer + decay constant uncertainty; (Fairchild et al., 2017)) is provided by an U-Pb date of a lava flow within the underlying Copper Harbor Conglomerate. Minor volcanics within the Freda Formation on the Keweenaw Peninsula are unlikely to be substantially younger than the youngest dated volcanics within the Midcontinent basin ( $1083.52 \pm 0.23/1.2$  Ma from the Michipicoten Island Formation; (Fairchild

et al., 2017)). An age of ca. 1080 Ma for the basal 500 meters of the Freda Formation is consistent with modeling of post-rift thermal subsidence (Hutchinson et al., 1990).

The studied intraclast-bearing outcrop is located along the Bad River (Copper Falls State Park, northern Wisconsin) in the lower portion of the Freda Formation – approximately 320 to 340 meters above its conformable base with the Nonesuch Formation (latitude: 46.3866°N, longitude 90.6373°W). The locality is contextualized in the context of regional geological data (Ontario Geological Survey, 2011; Nicholson et al., 2004; Jirsa et al., 2011; Ullman et al., 2015; Stewart & Mauk, 2017) in Text S1 and Figure S1. The two main lithofacies in the studied outcrop are: (1) siltstone to very fine sandstone with planar lamination and horizons of ripple cross-stratification and (2) coarse to very coarse subarkosic sandstone with dune-scale trough cross-stratification (Fig. 1). These lithofacies are consistent with a fluvial depositional environment where the coarse sandstone facies are channel deposits and the siltstones are inner-bank or over-bank deposits. The coarse-grained sandstone contains horizons of tabular cm-scale intraclasts comprised of the red siltstone lithology that is present in underlying beds of intact siltstone (Fig. 1). These tabular clayey-silt intraclasts were eroded within the depositional environment and redeposited in the sandstone. Due to migrating channels in fluvial systems, it is expected that a river will erode its own sediments. The intraclasts would have been held together through cohesion resulting from the clay component within the sediment. Given that the clasts are large (1 to 7 cm) relative to their host sediment, that they are angular, and that they would have been fragile at the time of deposition, it is unlikely that they were transported far within the channel.

## Paleomagnetic Results

Oriented samples were collected and analyzed from 39 Freda Formation intraclasts. The dimensions of the sampled clasts ranged from 2.2 x 1.4 x 0.5 cm to 7.2 x 2.3 x 1.2 cm. Given that the clasts were typically smaller than the 1-inch-diameter drill cores used for sampling, they were collected along with their sandstone matrix (Fig. S2). These oriented cores were mounted onto quartz glass discs with Omega CC cement and the matrix material was micro-drilled away. The quartz glass discs with Omega cement that has dried within a shielded room have magnetic moments of  $\sim 5E-11$  Am $^2$  while the clast natural remanent magnetizations (NRMs) have moments that are orders of magnitude stronger between 1.53E-08 and 5.74E-07 Am $^2$  (median of 1.34E-07 Am $^2$ ). The mounted clasts underwent stepwise thermal demagnetization in the UC Berkeley Paleomagnetism Lab using an ASC demagnetizer (residual fields <10 nT) with measurements made on a 2G DC-SQUID magnetometer. The demagnetization protocol had high resolution approaching the Neél temperature of hematite (5°C to 2°C to 1°C) resulting in 30 total thermal demagnetization steps (Fig. 2). All paleomagnetic data are available to the measurement level in the MagIC database (<https://earthref.org/MagIC/doi/10.1029/2018JB017067>).

The clasts typically reveal two distinct magnetization directions. One direction was similar throughout the intraclasts and was typically removed between 200°C and 650°C (Fig. 2). This mid-temperature component is continuously unblocked between these temperatures with no or minimal downward inflection at  $\sim 580^\circ\text{C}$  that would indicate appreciable remanence associated with magnetite (Fig. 2). This component is directionally well-grouped indicating that it was acquired following deposition of the clasts (Fig. 2, Table 1). The other component trends towards the origin and is removed by thermal demagnetization steps at the highest levels such that it typically can be fit by a least-squares line between 665°C and 688°C. The relative magnitude of the components varies between intraclasts (Fig. 2). While the high-temperature component can sometimes be fit as a line with a lower temperature bound of 660°C (BRIC.31a in Fig. 2), due to overlapping unblocking temperatures between the mid-temperature and high-temperature components, the lower bounds of the high-temperature fits sometimes need to be as high

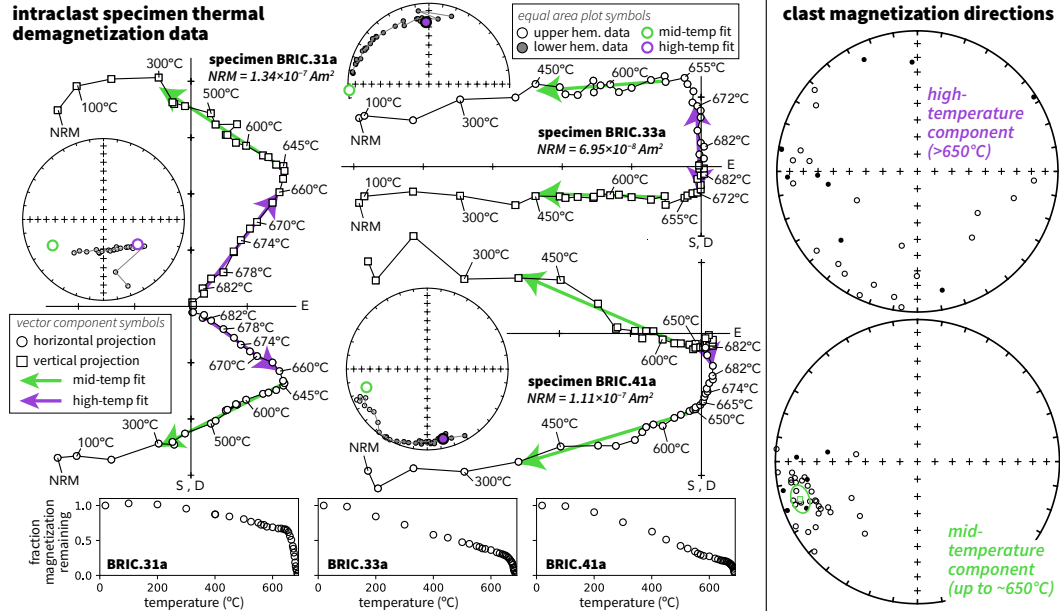


**Figure 2.** Paleomagnetic data from intraclasts reveal a mid-temperature component that typically unblocks prior to 655°C and a high-temperature component that typically unblocks between 655°C and 687°C. These components are present as varying fractions of the overall remanence as seen in the three individual clasts shown here on vector component plots and measurement-level equal area plots in tilt-corrected coordinates (developed using PmagPy; (Tauxe et al., 2016)). The direction of the mid-temperature component is shown as green arrows on the vector component plots and green circles on the equal area plots while the high-temperature component is shown with purple symbols. The mid-temperature component has a similar direction among the clasts as can be seen on the component directions equal area plots (tilt-corrected mean declination: 251.8, inclination: -12.4,  $\alpha_{95}$ : 6.6). In contrast, the high-temperature component directions are dispersed.

as 680°C (BRIC.41a in Fig. 2). Note that while the Néel temperature of hematite is sometimes reported as 675°C in the paleomagnetic literature, experimental data often show the Néel temperature to be as high as 690°C (Özdemir & Dunlop, 2006). In the data from the clasts, there is typically a significant directional change in the specimen magnetization between the mid-temperature component and the high-temperature component (Fig. 2). As a result, 30 of the 39 analyzed intraclast specimens could be fit with distinct mid-temperature and high-temperature least-squares lines. Note that the directions from one of these specimens (BRIC.4a) are not included in statistical calculations as its field orientation was uncertain. An additional seven specimens appear to be undergoing directional change through the highest thermal demagnetization steps suggesting the presence of a distinct high-temperature component, but this component was not well-expressed enough to be fit as a line. In contrast to the well-grouped mid-temperature component, the high-temperature component directions are dispersed, indicating that the component was acquired prior to erosion and redeposition of the clasts (Fig. 2). The high-temperature component directions are more dispersed in declination than inclination leading to a distribution that is not uniformly distributed on a sphere (Fig. 2). Given that the clasts are tabular, were liberated along their depositional lamination, and subsequently landed roughly bedding-parallel, it is to be expected that the rotations were largely around a vertical axis – preferentially changing declination. Due to this redeposition mechanism,

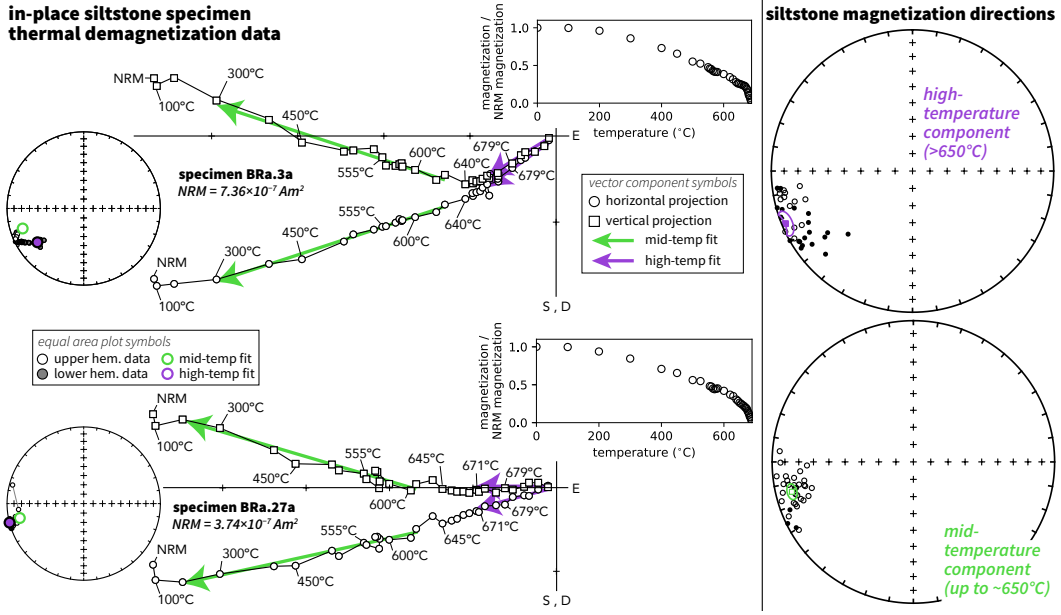


**Figure 3.** Paleomagnetic data from in-place siltstone beds reveal a mid-temperature component that typically unblocks prior to 655°C and a high-temperature component that typically unblocks between 655°C and 689°C. The direction of the mid-temperature component is shown as green arrows on the vector component plots and green circles on the equal area plots while the high-temperature component is shown with purple symbols. The mid-temperature component is similar to that removed from the clasts. The high-temperature component is well-grouped and has a distinct direction from the mid-temperature component with lower inclination.

it is expected that primary directions should be reoriented, but will not be randomly oriented. In the conglomerate test of (Watson, 1956), a resultant vector length of less than 8.7 is necessary to maintain the null hypothesis of randomness for  $n=29$ , while the resultant vector length for the high-temperature directions is 12.85. In addition to the tabular geometry, the clasts are quite large relative to the matrix (Fig. 1) which makes it unlikely that they were transported far – further limiting their dispersion. While the distribution is not random, the increased dispersion in the directions of well-resolved high-temperature components relative to the clast mid-temperature component and of the high-temperature component within in-place siltstone (Fig. 3) is consistent with the interpretation that the remanence rotated with the clasts.

In-place siltstone and very fine sandstone, representing the same lithologies that were liberated into intraclasts, were collected and analyzed following the same thermal demagnetization protocol. These samples were collected from a section stratigraphically below the intraclast-bearing outcrop along a small tributary creek to the Bad River (section BRa; latitude: 46.3852°N, longitude 90.6337°W). These samples are between 50 and 70 meters above the base of the Freda Formation within each sample collected at a distinct stratigraphic level. The thermally demagnetized specimens display very similar demagnetization behavior to the intraclasts with a mid-temperature component that progressively unblocks up to ~650°C and then transitions to a slightly different direction that unblocks up to ~689°C. The mid-temperature component from the insitu BRa samples and the mid-temperature component isolated from the intraclast samples share a common mean (Table 1). These mid-temperature component directional data sets pass both the bootstrap and Watson V tests for a common mean. The Watson V statistic of

**Table 1.** Summary of paleomagnetic directions

section (component)	n	dec	inc	$\alpha_{95}$	k	R
BRIC intraclasts (mid-temperature)	38	252.2	-14.4	6.5	13.9	35.33
BRIC intraclasts (high-temperature)	29				1.7	12.85
BRa in-place (mid-temperature)	33	256.2	-12.5	3.6	49.4	32.35
BRa in-place (high-temperature)	34	247.5	3.0	5.4	21.5	32.47

Notes: n—number of specimen fits included in the mean; dec—tilt-corrected mean declination in degrees; inc—tilt-corrected mean inclination in degrees;  $\alpha_{95}$ —95% confidence limit in degrees; k—Fisher precision parameter; R—resultant vector length. A bedding strike/dip of  $211^\circ/73^\circ$  was used for the tilt-correction of both BRIC and BRa directions. Given the dispersion in the intraclast high-temperature fits, the k and R values are given, but a mean direction is not shown.

2.0 is less than the critical value of 6.2 which implies that the null hypothesis that the two populations are drawn from distributions that share a common mean direction can not be rejected (Watson, 1983). The high-temperature component directions in the in-situ siltstones are well-grouped, in contrast to their dispersion between the intraclasts, and have a direction that is similar, but distinct, from the mid-temperature component. That the two populations are distinct is supported by bootstrap and Watson tests for a common mean (with a Watson V statistic of 45.6 which being greater than the critical value of 6.1 indicates the two means can be distinguished at the 95% confidence level). The inclination of the high-temperature component mean is very close to horizontal (Fig. 3, Table 1). The median angle difference between the mid-temperature and high-temperature components in the in-place siltstones is  $15^\circ$  in contrast to a larger median angle of  $46^\circ$  between the components in the reoriented clasts.

The paleomagnetic results on the in-place siltstone beds are similar to those obtained by Henry et al. (1977) who studied the basal Freda Formation in the Presque Isle Syncline and White Pine Basin of northern Michigan. As in our results, their data revealed a distinct mid-temperature component with a shallow upwards inclination and a high-temperature component with a near horizontal inclination. A progression from horizontal to upward inclinations is consistent with the expected change through time if the movement along the Keweenawan Track persisted past the end of rift magmatism (Fairchild et al., 2017; Swanson-Hysell et al., 2019) and is consistent with a later age of remanence acquisition for the mid-temperature component. While the inclination of the mid- and high-temperature components are indistinguishable between our data and that of Henry et al. (1977), the declinations are different such that their declinations are  $24^\circ$  more northerly than those obtained for BRa. The origin of this difference in declination is unclear and could be associated with complications in the tilt-correction such as non-cylindrical folding or multiple tilting episodes (inclination is relative to bedding tilt so would not be effected by such processes). It is premature to recalculate a paleomagnetic pole for the Freda Formation. More analyses are needed from the Freda Formation: 1) to evaluate this declination discrepancy; 2) develop enough directional data to robustly apply the elongation/inclination method for inclination flattening correction ( $>100$  to 150 samples necessary per (Tauxe et al., 2008)) to increase the quality of the paleomagnetic pole for the purposes of paleogeographic reconstruction and 3) expand data to span the stratigraphic thickness of the formation as current results are limited to the basal portion of the formation.

## Petrographic Results

Petrography on the intraclasts reveals two distinct populations of hematite (Fig. 1). One population is fine-grained pigmentary hematite present dominantly within the clay-sized matrix and rimming detrital silt-sized grains. The zones of pigmentary hematite within the matrix remain cloudy to high magnification indicating that the grains are sub-micron in size. The other population of hematite has similar sizes and shapes to other detrital silt-sized grains – typically ranging from 2 to 50  $\mu\text{m}$  in diameter. These hematite grains were identified through reflected light microscopy with their mineralogy supported by energy-dispersive x-ray spectroscopy conducted on a scanning electron microscope (SEM) at Lawrence Berkeley National Laboratory and confirmed by electron backscatter diffraction (EBSD) on an SEM at UC Berkeley (see Supporting Information Fig. S3 and Text S2 which contextualizes the results in the context of those of (Elmore & Van der Voo, 1982; Vincenz, 1968)).

## Rock Magnetic and Mössbauer Spectroscopy Results

The paleomagnetic data reveal that there are two distinct populations of remanence-carrying magnetic grains within the intraclasts and in-place siltstone with differing unblocking temperature ranges: one unblocking over a broad temperature range from 100°C up to 650°C or higher and the other dominantly unblocking between 665°C and 690°C. Rock magnetic experiments and Mössbauer spectroscopy can elucidate additional properties associated with the ferromagnetic mineralogy within the siltstone that is carrying the remanence as well as portions of the magnetic mineralogy that are not stable at room temperature.

Backfield demagnetization curves, where the specimens were pulsed in a 1.8 T field followed by a progressively larger field in the opposite direction, were developed on a Princeton Measurements vibrating sample magnetometer at the Institute for Rock Magnetism. Coercivity spectra, the derivative of the backfield curves, were modeled using the Max UnMix software package ((Maxbauer et al., 2016); Fig. 4). These spectra are well fit with two log-normal distributions associated with two populations of grains. One population has a median coercivity of  $\sim 300$  mT and a distribution that extends from the lowest to the highest coercivities (Fig. 4). The other population has a higher median coercivity of  $\sim 700$  mT and a coercivity distribution that is limited to the high coercivity range (Fig. 4). The high-coercivity phase can be considered to correspond with the plateau of high coercivities observed for single-domain hematite in the  $\sim 100$  nm to  $\sim 10 \mu\text{m}$  range (Özdemir & Dunlop, 2014). The spread in coercivities associated with the lower coercivity population is consistent with these values down to those associated with finer-grained hematite; the coercivity of hematite becomes progressively lower for grains that are smaller than 300 nm in diameter (Özdemir & Dunlop, 2014).

The frequency and temperature dependence of magnetic susceptibility was determined through experiments conducted on a Magnetic Properties Measurement System (MPMS) at the Institute for Rock Magnetism. The dependence of susceptibility on both temperature and frequency provides a sensitive and diagnostic means of characterizing magnetic nanoparticles (Worm & Jackson, 1999). We observe a frequency dependence of susceptibility that persists from 300 K down to 10 K (Fig. 5). This frequency dependence can be attributed to viscous superparamagnetic grains whose magnetic viscosity has relaxation times comparable to the AC field reversal interval (Worm, 1998; Worm & Jackson, 1999). This interpretation is supported by the frequency dependence of the in-phase susceptibility and the shared peak between the out-of-phase (quadrature) susceptibility and the  $\pi/2$  law ((Mullins & Tite, 1973); Fig. 5). That the frequency dependence extends across the full low-temperature range indicates a broad blocking temperature spectrum of viscous superparamagnetic grains associated with a wide size distribution of nanoparticles.

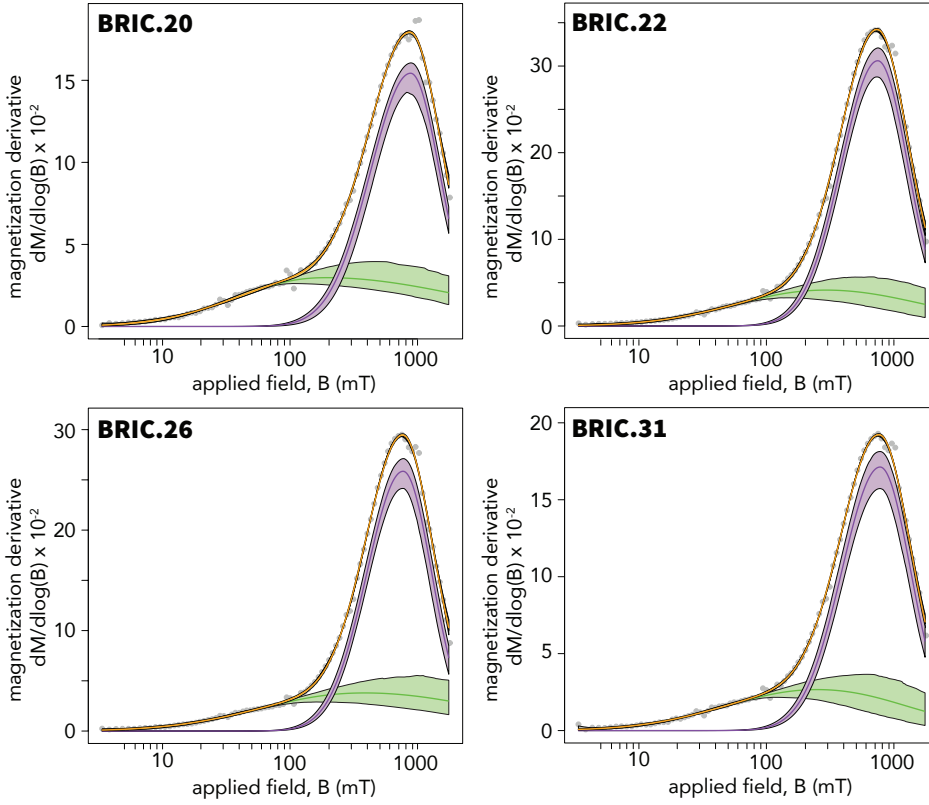


**Figure 4.** Coercivity spectra developed from backfield demagnetization curves on BRIC intraclast specimens with the points being the data. The data were modeled using log-Gaussian distributions implemented with the Max UnMix software package (Maxbauer et al., 2016). The coercivity spectra can be well-explained with two distributions: the higher coercivity distribution in purple and the lower coercivity distribution in green. The shaded areas represent 95% confidence intervals for the modeled components.

Hysteresis loops were measured from 5 T to -5 T on the MPMS (4020 field measurements per loop) at varying temperatures from room temperature (300 K) down to 50 K (Fig. 6). These low-temperature hysteresis data reveal a progressive increase in remanent magnetization ( $M_r$ ) as temperature decreases (Fig. 6) leading to  $M_r$  values that are between 9 and 13% higher at 50 K than at 300 K. This increase in  $M_r$  at low temperatures is likely associated with superparamagnetic grains transitioning to behave as stable single domain grains at lower temperature. There is also an increase in saturation magnetization ( $M_s$ ) as temperature decreases (Fig. 6). However, the hysteresis loops require subtraction of a large paramagnetic component that becomes progressively non-linear at low temperatures leading to the possibility that this increase in  $M_s$  is an artefact rather than an aspect of the ferromagnetic mineralogy of the samples. This increase in  $M_r$  is insensitive to this correction and is therefore a more robust feature of the data.

Mössbauer spectra were collected at the Institute for Rock Magnetism on bulk powders of intraclast samples at 300 K and 18 K (Fig. 7). The main feature of these spectra is a magnetically split sextet with a magnetic hyperfine field of about 51.6 T – diagnostic of hematite (Dyar et al., 2006). Modeling of the spectra reveal that the majority of iron within the samples resides within hematite (58% at 300 K and 60% at 18 K). Due to the high-frequency of Mössbauer spectroscopy, grains that are observed to be su-

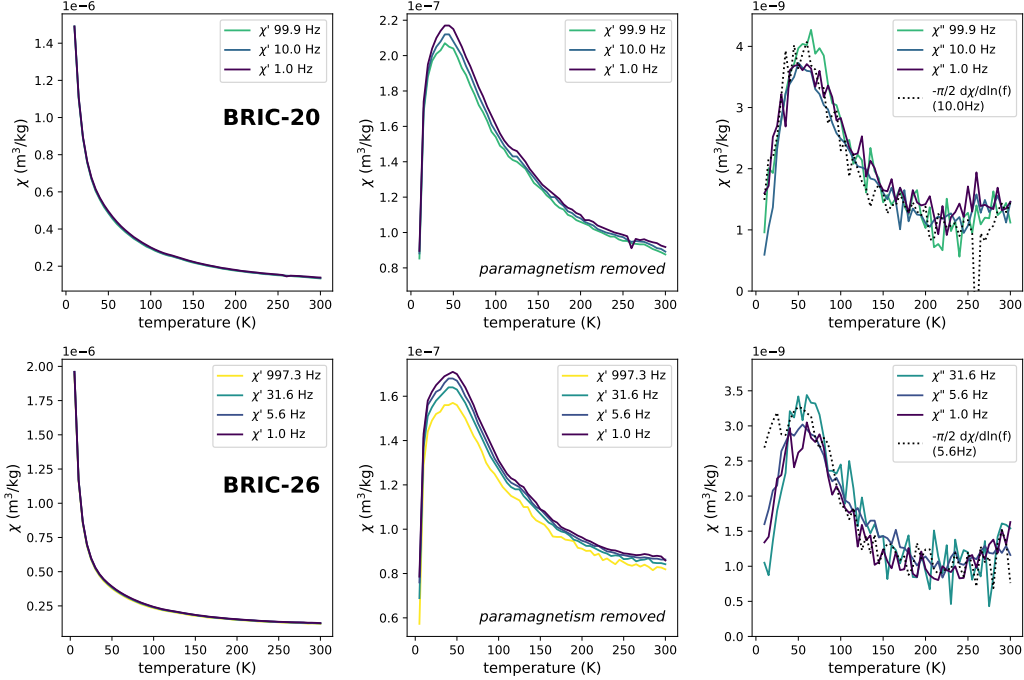


**Figure 5.** Frequency and temperature dependence of magnetic susceptibility ( $\chi$ ) for BRIC-20 and BRIC-26 from 10 to 300 K. The left panels show the in-phase susceptibility which is dominated by the paramagnetic component of the samples. In the middle panels, this paramagnetic component has been removed by creating a Curie-Weiss law model and subtracting it from the in-phase susceptibility data. Strong frequency dependence over the whole temperature range suggests a broad size distribution of nanoparticles (e.g. (Jackson & Swanson-Hysell, 2012)). The right panels show the out-of-phase (quadrature) susceptibility as well as the  $\pi/2$  relationship of  $\chi''[\text{viscosity}] = -(\pi/2)(\partial\chi'/\partial\ln(f))$  where  $f=\text{frequency}$ . These data document the presence of viscous superparamagnetic particles.

perparamagnetic at room temperature in typical rock magnetic experiments behave as stable ordered grains in Mössbauer spectra. Nevertheless, there is a slight increase in the magnitude of the hematite sextet relative to the doublets in the 18 K spectrum, leading to the slight increase in modeled hematite content, likely associated with ordering of the smallest nanoparticles of hematite ((Bødker et al., 2000); Fig. 7).

## DISCUSSION

Single-domain hematite grains have high coercivities ( $>150$  mT; (Özdemir & Dunlop, 2014)) and high unblocking temperatures. As a result, populations of hematite within rocks are stable on long timescales, resistant to overprinting, and therefore attractive for paleomagnetic study. In contrast to magnetite, hematite grains can retain stable single-domain behavior in crystals  $>1 \mu\text{m}$  with the threshold to multidomain behavior occurring in well-crystalline hematite when grain diameters exceed  $\sim 100 \mu\text{m}$  (Kletetschka & Wasilewski, 2002; Özdemir & Dunlop, 2014). Hematite nanoparticles with diameters less than  $\sim 30$  nm have superparamagnetic behavior wherein thermal fluctuation energy overwhelms the ability of the grain to retain a stable magnetization at Earth surface temperatures (Özdemir & Dunlop, 2014). Given the scatter associated with experimental data (Fig. 8), the diameter associated with the superparamagnetic to stable single do-

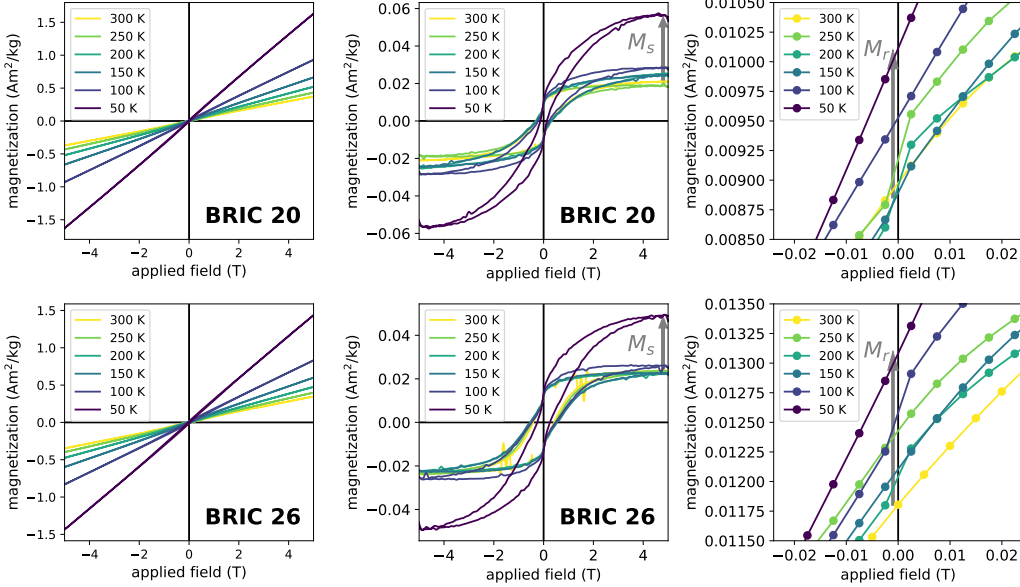


**Figure 6.** Hysteresis loops measured from room temperature (300 K) down to 50 K for silt-stone intraclast samples. The left panels are the raw uncorrected loops, the center panels remove the paramagnetic contribution using the methods of Jackson and Solheid (2010) and the right panels zoom-in on applied fields close to 0 to illustrate the progressive increase in remanent magnetization ( $M_r$ ) as temperature decreases.

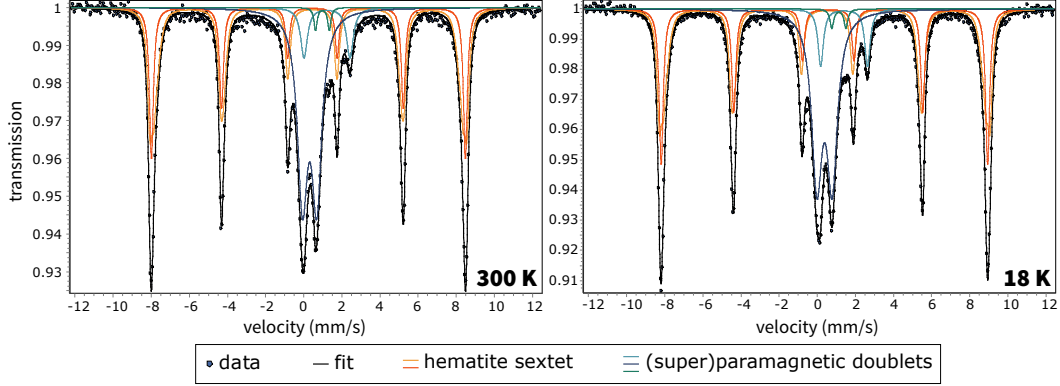


**Figure 7.** Mössbauer spectra developed at room temperature (300 K) and low temperature (18 K) on a powder of intraclast sample BRIC.22. Data are shown as dots with the black line representing a model fit. The sextet portion of the fit is shown with the red and yellow curves (representing the spread in hyperfine splitting resulting from a natural population) and is diagnostic of hematite. The central peak is comprised of doublets dominated by  $\text{Fe}^{3+}$ . The height of the hematite sextet relative to the central peak is slightly higher in the low temperature experiment likely due to ordering of the smallest hematite nanoparticles.

main transition is slightly uncertain, but is on the order of 10s of nm (Özdemir & Dunlop, 2014). Regardless, hematite grains become progressively less influenced by thermal fluctuations as they reach grain sizes of a few hundred nanometers at which point they are stable up to temperatures approaching the Néel temperature of  $\sim 685^\circ\text{C}$  (Swanson-

Hysell et al., 2011; Özdemir & Dunlop, 2014). As a result, there is a strong relationship between grain volume and unblocking temperature that can be utilized to estimate grain size following Néel relaxation theory (Néel, 1949; Swanson-Hysell et al., 2011). A hematite population that is progressively unblocking at thermal demagnetization steps well below the Néel transition temperature, such as the mid-temperature component of the intraclasts, is comprised of grains within the ~30 to ~400 nm size range (Fig. 8). This fine-grain size is consistent with the pigmentary phase observed within the intraclasts (Fig. 1).

Given the directional consistency of the mid-temperature component among the intraclasts (Fig. 2), this component must have dominantly formed as a chemical remanent magnetization after the intraclasts were redeposited in the channel. Chemical remanent magnetization acquisition by pigmentary hematite would have occurred as hematite grains grew to sizes above the superparamagnetic to stable single-domain transition resulting in the wide range of unblocking temperatures that is observed. The frequency dependence of susceptibility (Fig. 5) and increase in remanent magnetization following saturation at low-temperature (Fig. 6) both indicate the presence of a population of superparamagnetic grains. The coercivity spectra are consistent with a population of hematite that has a wide coercivity range extending from low coercivities up to high coercivities (the green component in the unmixing models of Fig. 4). Taken together, and compared to the hematite coercivity compilation of (Özdemir & Dunlop, 2014), these data indicate that a population of authigenic hematite nanoparticles that spans from <30 nm to >300 nm is responsible for the post-depositional chemical remanent magnetization (Fig. 8).

In contrast, the sharp unblocking temperature close to the Néel temperature of the high-temperature component indicates that it is dominantly held by hematite grains that are >400 nm (based on Néel relaxation theory; Fig. 8) such as the silt-sized hematite grains observed petrographically (Fig. 1). The high-coercivity population within the coercivity spectra (purple curves in Fig. 4) are consistent with this grain-size interpretation (Fig. 8). The high-temperature remanence component held by these grains was rotated along with the clasts indicating that it is primary and was acquired prior to the redeposition of the cohesive silt clasts. That this component is held by larger grain sizes supports it being a detrital remanent magnetization, rather than a chemical remanent magnetization that formed very early prior to clast erosion.

Detailed rock magnetic data through the Nonesuch Formation, which immediately underlies the Freda Formation, reveal that the lacustrine lithologies preserve a depth-dependent environmental magnetic signature where the deep water facies have no hematite in contrast to hematite-rich shallow water facies in sediments of similar grain size (Slotznick et al., 2018). This difference was interpreted by Slotznick et al. (2018) as being due to microbial reductive dissolution of iron oxides at low oxygen levels in the deepest part of the lake and oxidation of the detrital input in the shallowest part of the lake. Sediment that was deposited at intermediate water depths within the lake contains both detrital magnetite and hematite with minimal evidence for post-depositional reduction or oxidation leading to an interpretation of intermediate oxygen levels (Slotznick et al., 2018). That this depth-dependent relationship is consistent over significant length scales across the Midcontinent Rift basin indicates that hematite formation in those sediments, and likely the Freda Formation as well, is associated with redox conditions at the time of deposition rather than the subsequent migration of fluids. Oxidation of iron in surface environments often begins with the formation of fine-grained poorly crystalline ferrihydrite, which transforms to stable crystalline hematite at neutral pH on geologically short timescales (Cudennec & Lecerf, 2006; Jiang et al., 2018). The broad unblocking temperatures we observe for the chemical remanent magnetization in the Freda intraclasts are similar to those in hematite populations produced through experimental ferrihydrite to hematite conversion (Jiang et al., 2015). The direction of this chemical remanence is distinct, but

similar, to that of the detrital remanence with a change in both declination and inclination. This result suggests that the chemical remanence was acquired as plate motion continued at the end of the Keweenawan Track (Swanson-Hysell et al., 2019). This chemical remanent magnetization direction is well-grouped (Fig. 3) suggesting that the hematite that carries the remanence formed at a similar time rather than over a protracted period (which could lead to a streaked distribution; (Beck et al., 2003)). One possibility is that the conversion from a phase associated with the ferrihydrite to hematite transition that formed in the sediments in the near-surface was thermally activated by the geothermal gradient as the sediments were buried. More than 4 km of Freda Formation sediments were deposited atop those investigated in this study within the thermally subsiding basin that would have led to protracted interval at temperatures  $>100^{\circ}\text{C}$  following deposition. Such thermal activation of the transition of ferrihydrite, and/or intermediary phases such as hydromaghemite, to hematite could explain the association of chemical remanence directions with burial within the Midcontinent Rift. This mechanism could also explain the association of authigenic hematite remanence with other types of tectonothermal events such as the well-documented syn-folding chemical remanence of the Mauch Chunk Formation that is associated with the Alleghanian orogeny (Kent & Opdyke, 1985; Opdyke & DiVenere, 2004).

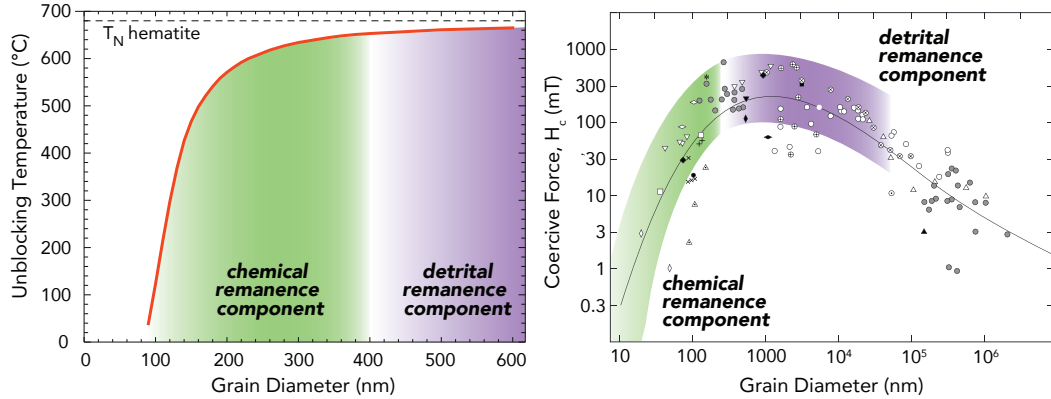


**Figure 8.** Left: Calculated unblocking temperatures using Néel thermal relaxation theory of idealized spherical hematite grains using a thermal fluctuation rate of  $10^{10} \text{ s}^{-1}$  and a relaxation time of 5 minutes for comparison to thermal demagnetization data (modified from (Swanson-Hysell et al., 2011)). The unblocking temperatures of the mid-temperature chemical component (green) and the high-temperature detrital component (purple) are shown and can be used to infer grain size. The Néel transition temperature ( $T_N$ ) is shown with a dashed line. Right: Compilation of coercivity data from hematite as a function of grain diameter from (Özdemir & Dunlop, 2014). The higher coercivity population from Fig. 4 corresponds to the larger grain sizes than the lower coercivity component associated with the chemical remanence.

The differential unblocking temperature spectra of the two components within the Freda intraclasts provides strong support for the argument of Jiang et al. (2015) that chemical and detrital remanent magnetization can be distinguished due to detrital remanence unblocking at the highest temperatures. However, the Freda intraclast data also show that while the detrital remanent magnetization can be well-isolated at temperatures as low as  $650^{\circ}\text{C}$  (specimen BRIC.31a in Fig. 2), the chemical remanent magnetization thermal unblocking spectra can overlap with that of the detrital remanence and extend up to temperatures closer to the Néel temperature (specimen BRIC.41a in Fig. 2). Therefore, to isolate primary remanence in red beds, best practice should be to proceed with very high resolution thermal demagnetization steps above  $600^{\circ}\text{C}$ , and partic-

ularly above 650°C. Characteristic remanence magnetization directions associated with hematite that are fit to components that span a wide range of unblocking temperatures including those lower than ~650°C are likely convolving a pigmentary chemical remanence and a detrital remanence held by larger grains.

A complication with detrital remanent magnetization is associated inclination-shallowing – an issue that has been explored in depth within the literature as pertains to hematite (e.g. (Tauxe & Kent, 1984; Iosifidi et al., 2010; Bilardello & Kodama, 2010b)). The presence of both pigmentary and detrital hematite complicates efforts that seek to use bulk magnetic fabrics to correct for these effects. This reality necessitates the use of careful methodologies that target the fabric of only the highest-unblocking-temperature hematite (e.g. (Bilardello, 2015)) or that take other approaches such as analyzing the elongation of the directional distribution and correcting to values taken from secular variation models (the elongation-inclination method of (Tauxe & Kent, 2004)).

Hematite-bearing sedimentary rocks have varied characteristics which has lead to the argument that it is difficult to apply results from red beds in one formation to those from another. However, the rock magnetic properties of the hematite grain size distributions that emerge from these data are associated with their mode of incorporation into the sediment. Hydrodynamic sorting associated with the delivery of detrital hematite will lead to a narrower and coarser size distribution of grains than that of authigenic pigmentary hematite growth. Authigenic growth can lead to a distribution of grains that span from sub-30 nm superparamagnetic grains up to stable single-domain grains >300 nm in diameter. Such an authigenic population has distinct rock magnetic characteristics including a very broad coercivity distribution and viscous superparamagnetic grains that can be detected through low-temperature magnetometry.

Overall, the intraclast data, combined with those of the in-place siltstone, reveal that directional change at the highest unblocking temperatures provides an effective means to discriminate primary and secondary magnetizations within siltstones of the Freda Formation. The isolation of remanence carried by primary detrital hematite in >1 billion-year-old siltstones lends confidence to magnetostratigraphic records and paleogeographic interpretations that are based on interpretations of primary magnetization isolated from high-unblocking-temperature hematite in ancient red beds.

### Acknowledgments

This research was supported by the Esper S. Larsen, Jr. Research Fund and the National Science Foundation through grant EAR-1419894. Rock magnetic experiments were conducted during an Institute for Rock Magnetism (IRM) visiting fellowship. The IRM and its visiting fellowship program is made possible through the Instrumentation and Facilities program of the National Science Foundation, Earth Science Division and funding from the University of Minnesota. SPS was supported by the Miller Institute for Basic Research in Science. The Wisconsin Department of Natural Resources granted a research and collection permit that enabled sampling within Copper Falls State Park. Oliver Abbit assisted with field work, Taiyi Wang assisted with paleomagnetic analyses and Tim Teague provided technical support for EBSD analyses. Peat Solheid, Mike Jackson, and Dario Bilardello provided technical support at the Institute for Rock Magnetism. Discussions with them, and with Josh Feinberg and Bruce Moskowitz, provided insight on rock magnetic data interpretation. Reviews from Associate Editor Mark Dekkers, Dario Bilardello and an anonymous referee improved the manuscript. Data associated with this study are available within the MagIC database (<https://earthref.org/MagIC/doi/10.1029/2018JB017067>) and a Github repository associated with this work ([https://github.com/Swanson-Hysell-Group/2019\\_Red\\_Bed\\_Intraclasts](https://github.com/Swanson-Hysell-Group/2019_Red_Bed_Intraclasts)) which is also archived on Zenodo (<https://doi.org/10.5281/zenodo.2641335>). The Github repository also contains Python code related to calculations, visualizations and statistical tests discussed herein.

## References

- Beck, M. E., Burmester, R. F., & Housen, B. A. (2003). The red bed controversy revisited: shape analysis of Colorado Plateau units suggests long magnetization times. *Tectonophysics*, 362(1-4), 335–344. doi: 10.1016/s0040-1951(02)00644-3
- Bilardello, D. (2015). Isolating the anisotropy of the characteristic remanence-carrying hematite grains: a first multispecimen approach. *Geophysical Journal International*, 202(2), 695–712. doi: 10.1093/gji/ggv171
- Bilardello, D., & Kodama, K. P. (2010a). Palaeomagnetism and magnetic anisotropy of Carboniferous red beds from the Maritime Provinces of Canada: evidence for shallow palaeomagnetic inclinations and implications for North American apparent polar wander. *Geophysical Journal International*, 180(3), 1013–1029. doi: 10.1111/j.1365-246x.2009.04457.x
- Bilardello, D., & Kodama, K. P. (2010b). Rock magnetic evidence for inclination shallowing in the early Carboniferous Deer Lake Group red beds of western Newfoundland. *Geophysical Journal International*, 181(1), 275–289. doi: 10.1111/j.1365-246x.2010.04537.x
- Bødker, F., Hansen, M. F., Koch, C. B., Lefmann, K., & Mørup, S. (2000). Magnetic properties of hematite nanoparticles. *Physical Review B*, 61(10), 6826–6838. doi: 10.1103/physrevb.61.6826
- Butler, R. (1992). *Paleomagnetism: Magnetic domains to geologic terranes*. Blackwell Scientific Publications.
- Cannon, W. F. (1992). The Midcontinent rift in the Lake Superior region with emphasis on its geodynamic evolution. *Tectonophysics*, 213(1-2), 41–48. doi: 10.1016/0040-1951(92)90250-A
- Collinson, D. W. (1965). Origin of remanent magnetization and initial susceptibility of certain red sandstones. *Geophysical Journal International*, 9(2-3), 203–217. doi: 10.1111/j.1365-246x.1965.tb02071.x
- Cudennec, Y., & Lecerf, A. (2006). The transformation of ferrihydrite into goethite or hematite, revisited. *Journal of Solid State Chemistry*, 179(3), 716–722. doi: 10.1016/j.jssc.2005.11.030
- DiVenere, V. J., & Opdyke, N. D. (1991). Magnetic polarity stratigraphy in the uppermost Mississippian Mauch Chunk Formation, Pottsville, Pennsylvania. *Geology*, 19(2), 127. doi: 10.1130/0091-7613(1991)019<127:mpsitu>2.3.co;2
- Dyar, M. D., Agresti, D. G., Schaefer, M. W., Grant, C. A., & Sklute, E. C. (2006). Mössbauer spectroscopy of earth and planetary materials. *Annual Review of Earth and Planetary Sciences*, 34(1), 83–125. doi: 10.1146/annurev.earth.34.031405.125049
- Elmore, R. D., & Van der Voo, R. (1982). Origin of hematite and its associated remanence in the Copper Harbor Conglomerate (Keweenawan), upper Michigan. *J. Geophys. Res.*, 87(B13), 10918–10928. doi: 10.1029/JB087iB13p10918
- Fairchild, L. M., Swanson-Hysell, N. L., Ramezani, J., Sprain, C. J., & Bowring, S. A. (2017). The end of Midcontinent Rift magmatism and the paleogeography of Laurentia. *Lithosphere*, 9(1), 117–133. doi: 10.1130/L580.1
- Henry, S., Mauk, F., & Van der Voo, R. (1977). Paleomagnetism of the upper Keweenawan sediments: Nonesuch Shale and Freda Sandstone. *Canadian Journal of Earth Science*, 14, 1128–1138. doi: 10.1139/e77-103
- Hutchinson, D., White, R., Cannon, W., & Schulz, K. (1990). Keweenaw hot spot: Geophysical evidence for a 1.1 Ga mantle plume beneath the Midcontinent Rift System. *Journal of Geophysical Research: Solid Earth*, 95(B7), 10869–10884. doi: 10.1029/jb095ib07p10869
- Iosifidi, A. G., Mac Niocaill, C., Khrarov, A. N., Dekkers, M. J., & Popov, V. V. (2010, Jul). Palaeogeographic implications of differential inclination shallowing in Permo-Carboniferous sediments from the Donets Basin, Ukraine. *Tectonophysics*, 490(3-4), 229–240. doi: 10.1016/j.tecto.2010.05.017

- Jackson, M., & Solheid, P. (2010). On the quantitative analysis and evaluation of magnetic hysteresis data. *Geochem. Geophys. Geosyst.*, 11(4). doi: 10.1029/2009GC002932
- Jackson, M., & Swanson-Hysell, N. (2012). Rock magnetism of remagnetized carbonate rocks: Another look. In R. Elmore (Ed.), *Remagnetization and chemical alteration of sedimentary rocks* (Vol. 371). Geological Society London, Special Publications. doi: 10.1144/SP371.3
- Jiang, Z., Liu, Q., Dekkers, M. J., Tauxe, L., Qin, H., Barrón, V., & Torrent, J. (2015, Oct). Acquisition of chemical remanent magnetization during experimental ferrihydrite–hematite conversion in earth-like magnetic field—implications for paleomagnetic studies of red beds. *Earth and Planetary Science Letters*, 428, 1–10. doi: 10.1016/j.epsl.2015.07.024
- Jiang, Z., Liu, Q., Dekkers, M. J., Zhao, X., Roberts, A. P., Yang, Z., ... Liu, J. (2017). Remagnetization mechanisms in Triassic red beds from South China. *Earth and Planetary Science Letters*, 479, 219–230. doi: 10.1016/j.epsl.2017.09.019
- Jiang, Z., Liu, Q., Roberts, A. P., Barrón, V., Torrent, J., & Zhang, Q. (2018). A new model for transformation of ferrihydrite to hematite in soils and sediments. *Geology*. doi: 10.1130/g45386.1
- Jirsa, M. A., Boerboom, T., Chandler, V., Mossler, J., Runkel, A., & Setterholm, D. (2011). *S-21 Geologic map of Minnesota-bedrock geology* (Tech. Rep.). Minnesota Geological Survey. Retrieved from <http://hdl.handle.net/11299/101466>
- Kent, D. V., & Opdyke, N. D. (1985). Multicomponent magnetizations from the mississippian mauch chunk formation of the central appalachians and their tectonic implications. *Journal of Geophysical Research: Solid Earth*, 90(B7), 5371–5383. doi: 10.1029/jb090ib07p05371
- Kirschvink, J. (1980). The least-squares line and plane and the analysis of paleomagnetic data. *Geophysical Journal of the Royal Astronomical Society*, 62(3), 699–718. doi: 10.1111/j.1365-246x.1980.tb02601.x
- Kletetschka, G., & Wasilewski, P. J. (2002). Grain size limit for SD hematite. *Physics of the Earth and Planetary Interiors*, 129, 173–179. doi: 10.1016/S0031-9201(01)00271-0
- Larson, E. E., & Walker, T. R. (1982). A rock magnetic study of the lower massive sandstone, Moenkopi Formation (Triassic), Gray Mountain Area, Arizona. *Journal of Geophysical Research: Solid Earth*, 87(B6), 4819–4836. doi: 10.1029/jb087ib06p04819
- Liebes, E., & Shive, P. N. (1982). Magnetization acquisition in two Mesozoic red sandstones. *Physics of the Earth and Planetary Interiors*, 30(4), 396–404. Retrieved from [http://dx.doi.org/10.1016/0031-9201\(82\)90049-8](http://dx.doi.org/10.1016/0031-9201(82)90049-8) doi: 10.1016/0031-9201(82)90049-8
- Maxbauer, D. P., Feinberg, J. M., & Fox, D. L. (2016). MAX UnMix: A web application for unmixing magnetic coercivity distributions. *Computers and Geosciences*, 95, 140–145. doi: 10.1016/j.cageo.2016.07.009
- Molina-Garza, R. S., Geissman, J. W., Voo, R. V. d., Lucas, S. G., & Hayden, S. N. (1991). Paleomagnetism of the Moenkopi and Chinle Formations in central New Mexico: Implications for the North America apparent polar wander path and triassic magnetostratigraphy. *Journal of Geophysical Research*, 96, 14239–14262. doi: 10.1029/91JB00644
- Mullins, C. E., & Tite, M. S. (1973). Magnetic viscosity, quadrature susceptibility, and frequency dependence of susceptibility in single-domain assemblies of magnetite and maghemite. *Journal of Geophysical Research*, 78(5), 804–809. doi: 10.1029/jb078i005p00804
- Néel, L. (1949). Théorie due trainage magnétique des ferromagnétiques en grains fins avec applications au terres cuites. *Annales de Géophysique*, 5(99).

- Nicholson, S. W., Dicken, C. L., Foose, M. P., & Mueller, J. A. L. (2004). *Preliminary integrated geologic map databases for the United States: Minnesota, Wisconsin, Michigan, Illinois, and Indiana* (U.S. Geological Survey Open-File Report). U.S. Geological Survey. Retrieved from <http://pubs.usgs.gov/of/2004/1355/>
- Ojakangas, R. W., Morey, G. B., & Green, J. C. (2001). The Mesoproterozoic Mid-continent Rift System, Lake Superior Region, USA. *Sedimentary Geology*, 141-142, 421–442. doi: 10.1016/s0037-0738(01)00085-9
- Ontario Geological Survey. (2011). *1:250 000 scale bedrock geology of Ontario, Miscellaneous Release—Data 126-Revision 1* (Tech. Rep.). Ontario Geological Survey.
- Opdyke, N. D., & DiVenere, V. J. (2004). The magnetic polarity stratigraphy of the Mauch Chunk Formation, Pennsylvania. *Proceedings of the National Academy of Sciences*, 101(37), 13423–13427. doi: 10.1073/pnas.0403786101
- Özdemir, Ö., & Dunlop, D. J. (2006). Magnetic memory and coupling between spin-canted and defect magnetism in hematite. *J. Geophys. Res.*, 111(B12). doi: 10.1029/2006JB004555
- Özdemir, Ö., & Dunlop, D. J. (2014). Hysteresis and coercivity of hematite. *Journal of Geophysical Research: Solid Earth*, 119(4), 2582–2594. doi: 10.1002/2013JB010739
- Purucker, M. E., Elston, D. P., & Shoemaker, E. M. (1980). Early acquisition of characteristic magnetization in red beds of the Moenkopi Formation (Triassic), Gray Mountain, Arizona. *Journal of Geophysical Research*, 85(B2), 997. doi: 10.1029/jb085ib02p00997
- Slotznick, S. P., Swanson-Hysell, N. L., & Sperling, E. A. (2018). Oxygenated mesoproterozoic lake revealed through magnetic mineralogy. *Proceedings of the National Academy of Sciences*. doi: 10.1073/pnas.1813493115
- Stewart, E. K., & Mauk, J. L. (2017, 6). Sedimentology, sequence-stratigraphy, and geochemical variations in the Mesoproterozoic Nonesuch Formation, northern Wisconsin, USA. *Precambrian Research*, 294, 111–132. Retrieved from <http://www.sciencedirect.com/science/article/pii/S0301926816302297> doi: 10.1016/j.precamres.2017.03.023
- Swanson-Hysell, N. L., Feinberg, J. M., Berqué, T. S., & Maloof, A. C. (2011). Self-reversed magnetization held by martite in basalt flows from the 1.1-billion-year-old Keweenawan rift, Canada. *Earth and Planetary Science Letters*, 305(1-2), 171–184. doi: 10.1016/j.epsl.2011.02.053
- Swanson-Hysell, N. L., Ramezani, J., Fairchild, L. M., & Rose, I. R. (2019, Jan). Failed rifting and fast drifting: Midcontinent rift development, Laurentia's rapid motion and the driver of Grenvillian orogenesis. *GSA Bulletin*. Retrieved from <http://dx.doi.org/10.1130/B31944.1> doi: 10.1130/b31944.1
- Tauxe, L., & Kent, D. (1984). Properties of a detrital remanence carried by hematite from study of modern river deposits and laboratory redeposition experiments. *Geophysical Journal of the Royal Astronomical Society*, 77, 543–561. doi: 10.1111/j.1365-246X.1984.tb01909.x
- Tauxe, L., & Kent, D. (2004). A simplified statistical model for the geomagnetic field and the detection of shallow bias in paleomagnetic inclinations: was the ancient magnetic field dipolar? In J. Channell, D. Kent, W. Lowrie, & J. Meert (Eds.), *Timescales of the paleomagnetic field* (Vol. 145, p. 101–116). American Geophysical Union. doi: 10.1029/145GM08
- Tauxe, L., Kent, D. V., & Opdyke, N. D. (1980). Magnetic components contributing to the NRM of Middle Siwalik red beds. *Earth and Planetary Science Letters*, 47, 279–284. doi: 10.1016/0012-821X(80)90044-8
- Tauxe, L., Kodama, K., & Kent, D. (2008). Testing corrections for paleomagnetic inclination error in sedimentary rocks: A comparative approach. *Physics of the Earth and Planetary Interiors*, 169(1-4), 152–165. doi: 10.1016/j.pepi.2008.05

.006

- Tauxe, L., Shaar, R., JonesTrask, L., Swanson-Hysell, N., Minnett, R., Koppers, A., ... Fairchild, L. (2016). PmagPy: Software package for paleomagnetic data analysis and a bridge to the Magneetics Information Consortium (MagIC) Database. *Geochemistry, Geophysics, Geosystems*. doi: 10.1002/2016GC006307
- Ullman, D. J., Carlson, A. E., LeGrande, A. N., Anslow, F. S., Moore, A. K., Caffee, M., ... Licciardi, J. M. (2015, Jan). Southern Laurentide ice-sheet retreat synchronous with rising boreal summer insolation. *Geology*, 43(1), 23–26. Retrieved from <http://dx.doi.org/10.1130/G36179.1> doi: 10.1130/g36179.1
- Van Der Voo, R., & Torsvik, T. H. (2012). The history of remagnetization of sedimentary rocks: deceptions, developments and discoveries. *Geological Society, London, Special Publications*, 371(1), 23–53. doi: 10.1144/SP371.2
- Van Houten, F. B. (1968). Iron oxides in red beds. *Geological Society of America Bulletin*, 79(4), 399. doi: 10.1130/0016-7606(1968)79[399:ioirb]2.0.co;2
- Vincenz, S. A. (1968). Phenomenon of partial self-reversal in Keweenawan rocks 1. magnetization of Portage Lake lavas. *Journal of Geophysical Research*, 73, 2729-2752.
- Watson, G. S. (1956). A test for randomness of directions. *Geophysical Journal International*, 7, 160-161. doi: 10.1111/j.1365-246X.1956.tb05561.x
- Watson, G. S. (1983, 12). Large sample theory of the Langevin distribution. *Journal of Statistical Planning and Inference*, 8(3), 245–256. doi: 10.1016/0378-3758(83)90043-5
- Worm, H.-U. (1998). On the superparamagnetic—stable single domain transition for magnetite, and frequency dependence of susceptibility. *Geophysical Journal International*, 133(1), 201-206. doi: 10.1046/j.1365-246X.1998.1331468.x
- Worm, H.-U., & Jackson, M. (1999). The superparamagnetism of Yucca Mountain Tuff. *J. Geophys. Res.*, 104(B11), 25415–25425. doi: 10.1029/1999JB900285